Pure appl. geophys. 162 (2005) 1–20
0033 – 4553/05/010001-20
DOI 10.1007/s00024-004-2576-4

Pure and Applied Geophysics

Observed Evolution of Linear and Nonlinear Effects at the Dahan Downhole Array, Taiwan: Analysis of the September 21, 1999 M 7.3 Chi-Chi Earthquake Sequence

HUEY-CHU HUANG,[1] SHIN-WEI HUANG,[1] and HUNG-CHIE CHIU[2]

Abstract — In this paper, the site characteristics of the Dahan downhole array are studied by analyzing the September 21, 1999 *M* 7.3 Chi-Chi earthquake sequence including the main shock and some aftershocks. The four-level array (0 m, 50 m, 100 m and 200 m) is located to the north of Hualien City in eastern Taiwan. Polarization analysis is used to check the orientation errors of the seismometers at different levels of depth. If the surface instrument is chosen as reference, the angle between the major polarization axes of the surface and any downhole records is the orientation error that must be corrected for the downhole accelerographs. The orientation errors at depths of 50 m, 100 m and 200 m are 32°, 120° and −84°. After the corrections, the coherency between the surface and downhole records is substantially improved. Spectral ratio analysis shows that the predominant frequency of the Chi-Chi main shock shifts to a lower frequency. We also simulate ground motions at different depths by using the Haskell method with a linear velocity structure model. The record at surface is chosen as the input motion. Compared with the observed data, ground acceleration can be well reproduced for the aftershocks (weak-motion events) of the September 21, 1999 *M* 7.3 Chi-Chi earthquake. However, for the Chi-Chi main shock, the synthetic waveform cannot match well with the observation neither in amplitude nor in phase. This indicates that large ground shaking probably induced the nonlinear site effect at that time, and the model used cannot support it.

Key words: Downhole array, Chi-Chi earthquake, polarization analysis, Haskell method, spectral ratio.

1. Introduction

Linear and nonlinear site effects have been examined in several studies (e.g., JOYNER and CHEN, 1975; YU *et al*., 1993; AGUIRRE and IRIKURA, 1995, 1997; NI *et al*., 1997). By and large, amplification of seismic waves originates from the strong contrast between the physical properties of rocks and sediments. To evaluate this amplification, the seismic response of the soil is treated as a linear behavior under low levels of strain. For larger stress-strain levels, however, the results of laboratory testing of soil samples show a nonlinear relation that represents the nonlinear character of the soil response.

[1] Institute of Applied Geophysics, National Chung Cheng University, Taiwan.
[2] Institute of Earth Sciences, Academia Sinica, Taiwan. E-mail: seihuey@eq.ccu.edu.tw

Certain authors have been trying to determine observational evidence of nonlinearity from seismological data and to estimate to what degree it influences strong ground motions (CHIN and AKI, 1991; BERESNEV *et al.*, 1995a; BERESNEV *et al.*, 1998a,b; SU *et al.*, 1998; CULTRERA *et al.*, 1999). In those studies, the nonlinear effect causes a reduction in waveform amplitude in the time domain and the shifting of predominant frequencies and peak reduction in the frequency domain. This is due to the nonlinear response of the material which brings about a change in the elastic properties of the medium dependent on waveform amplitudes. AGUIRRE and IRIKURA (1997) studied nonlinearity, liquefaction and velocity variation of soft soil layers in Port Island, Kobe, during the 1995 Hyogo-ken Nanbu earthquake. The *S*-wave velocity structure before and after the main shock was found to be different. More specifically, the *S*-wave velocity of the second layer (5 m to 16 m depths) after the main shock dropped some 20%. The liquefied state remained at least 3 hrs but not more than 24 hrs after the main shock. The strong influence of nonlinearity during the main shock yielded a significant reduction (25%) in the horizontal ground motions at the surface.

Several techniques have been used to detect the nonlinear effect. One is spectral ratio evaluation of observed data between surface and bedrock during strong and weak ground motions (ORDAZ and FACCIOLI, 1994; BERESNEV *et al.*, 1995a; HARTZELL, 1998; SU *et al.*, 1998). An alternative way of estimating the soil layer effect is to use recordings from a vertical array of seismometers (WEN *et al.*, 1994, 1995; AGUIRRE and IRIKURA, 1995; BERESNEV *et al.*, 1995b; SATOH *et al.*, 1995; ELGAMAL *et al.*, 1996; BORJA *et al.*, 1999, 2000). The reduction and/or shift in the peaks during strong motion are indications of nonlinearity. Another technique used to evaluate nonlinearity is based on the comparison of observed ground motions during strong motion with those simulated by a linear method. The difference from the observed data can be interpreted as nonlinearity. Two commonly used linear methods are the 1-D Haskell method and the empirical Green's function method (e.g., AKI and IRIKURA, 1991; AGUIRRE *et al.*, 1994). Numerical approaches to predict the nonlinear response of soil can be classified as either an equivalent secant approach (e.g., the SHAKE program by SCHNABEL *et al.,* 1972) or a direct nonlinear approach (e.g., the DESRA2 program by LEE and FINN 1982; the CHARSOIL program by STREETER *et al.,* 1974; and the SPECTRA program by BORJA and WU 1994).

The Chi-Chi earthquake ($M_L = 7.3$) struck the middle part of Taiwan on September 21, 1999, causing very extensive damage. It also triggered many strong-motion seismometers and produced many high-quality recordings. In this study, we study the site characteristics of the Dahan downhole array using the recordings of the Chi-Chi earthquake sequences. First, we examine the orientation errors of the downhole instruments at the depths of 50 m, 100 m and 200 m. In order to understand both the linear and nonlinear behavior of the soft soil layers, the spectral ratio is calculated by dividing the spectrum at surface relative to that at the depths of

50 m, 100 m and 200 m for the strong and weak motion events. Based on the shear-wave velocity structure by the uphole and cross-hole shooting methods, we simulate the Chi-Chi earthquake sequences including the main shock and aftershock events.

2. Dahan Downhole Array and Data

The Dahan downhole array (represented by the triangular symbol in Fig. 1) is located to the north of Hualien City in eastern Taiwan. Four triaxial downhole force-balance accelerometers (FBA-23D) were installed at the Dahan site in March 1992. These instruments are at the depths of 0 m (surface), 50, 100 and 200 m within a 3 m × 3 m area. A schematic cross section of the site, the deployment of instruments, geology and the velocity profiles of the *P* and *S* waves are shown in Figure 2. Based

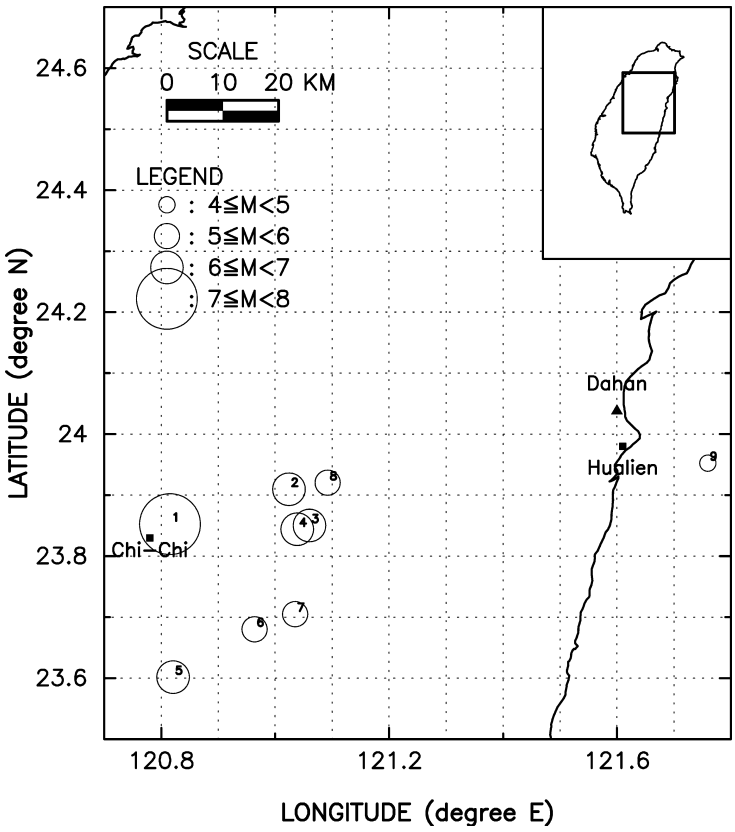

Figure 1
Site of the Dahan downhole accelerometer array, marked with a triangular symbol, is located in the Hualien area of Taiwan. Open circles represent the epicenters of the Chi-Chi earthquake sequences.

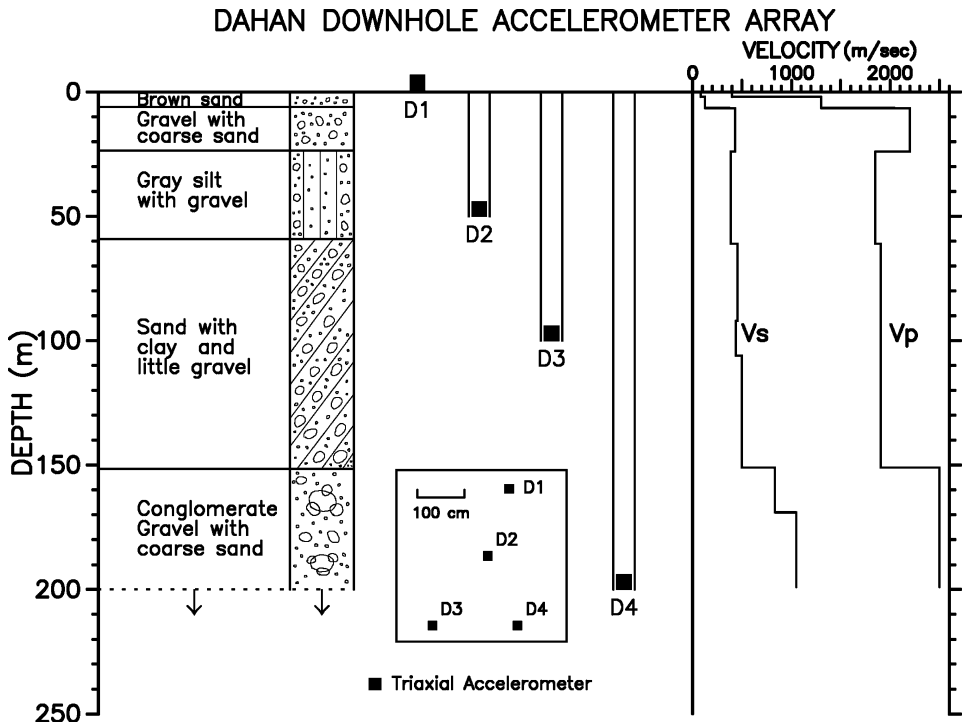

Figure 2
Four-level Dahan downhole accelerometer array and cross section of its geological strata, *S*-wave and *P*-wave velocities.

on the geology of the site, gravel is predominant except for alluvium deposits near the surface 0.5 m. Digital data were recorded as 16-bit words at the rate of 200 samples per second.

During a 16-month operation from September 1999 to December 2000, 68 earthquakes ($2.7 \leq M_L \leq 7.3$) triggered this array. We analyze nine of these in this paper. Figure 1 shows the epicentral locations of the earthquakes used. The relative ground motion parameters, PGA and PHV values, at the surface station for these nine earthquakes are tabulated in Table 1. The maximum PGA value is 230 gals recorded at the surface station (Event 1). In this site, the strong (with significant nonlinear effect) and weak (no noticeable nonlinear effect) motions can roughly be classified by the PGA at the free surface station. The thresholds for strong and weak motions at this site are 150 and 60 gals, respectively (WEN *et al.*, 1995). Events 2 and 4 in this data set fall between these two categories. However, the PGA value in this paper is used to roughly quantify earthquakes as weak and strong ones, and not to characterize the soil amplification.

Table 1

Source parameters of earthquakes used as recorded by the Dahan downhole array

Event No.		Original time (UT)	Latitude (°N)	Longitude (°E)	Depth (km)	M_L	Δ (km)	Back-Azimuth (degree)	PGA (cm/sec^2)	PHV (cm/sec)
1	S	1999/09/20 17:47	23.85	120.82	8.00	7.3	82.41	255.73	230	31.5
2		1999/09/20 17:57	23.91	121.02	2.23	6.47	60.23	256.46	87	8.8
3	S	1999/09/20 18:11	23.85	121.06	1.00	6.7	58.69	249.36	166	7.8
4		1999/09/20 18:16	23.84	121.04	1.10	6.66	60.99	249.51	68	4.8
5	W	1999/09/20 21:47	23.60	120.82	0.32	6.59	92.83	238.81	18	1.9
6	W	1999/09/25 08:43	23.68	120.96	6.86	5.85	75.85	238.66	25	1.8
7	W	1999/10/18 16:00	23.70	121.04	23.77	5.15	68.31	237.45	33	1.5
8	W	2000/06/19 21:56	23.92	121.09	27.02	5.18	53.29	255.94	21	1.2
9	W	2000/07/14 09:40	23.95	121.76	8.00	4.89	18.91	120.06	51	6.2

In the spectral ratio analysis, a 20-second window, which primarily brackets the large amplitude *S*-wave parts of the seismograms, is used with a 5% cosine taper. Fourier amplitudes are calculated for all accelerograms used. In order to avoid pseudo-peaks, a smoothing technique with a 0.25 Hz Hanning window is applied to the raw spectra, and subsequently spectral ratios are calculated. Based on recording quality and completeness, we choose nine events, including two strong-motion events (marked with "S" in Table 1), five weak-motion events (marked with "W" in Table 1) and two events with PGA values between 60 and 150 gals. Comparing the seismic signal and pre-event noise, all data have a signal-to-noise ratio larger than 10.

3. Orientation Errors of Downhole Instruments

CHIU *et al.* (1994) have previously estimated the orientation errors and the tilt of the downhole accelerometers at the Dahan site using polarization analysis. However, these seismometers malfunctioned in 1999. After being repaired, they were reinstalled, and their orientations still require further examination.

These downhole accelerometers recorded many excellent seismic data sets, including those of the main shock and its aftershocks when the Chi-Chi earthquake struck the middle part of Taiwan on September 21, 1999. In this paper, polarization analysis, particle-motion analysis and coherency functions are used to check the orientation errors of the seismometers at different depths. We estimated the orientation errors using some events and their results are similar. Here we only display the results of the 14 July 2000 earthquake (Event 9). Figure 3 shows the strike of maximum polarization axes as a function of time for the 14 July 2000 event. From top to bottom, they correspond to the surface, the 50, 100 and the 200 m accelerometers. Arrows mark the primary *S* arrivals, and the corresponding numbers signify the strikes in degrees. The window length for the analysis is 1 sec, and the window shift for each polarization analysis is 0.05 sec. If the surface instrument is chosen as the reference, the angle between the major polarization axes of the surface and any downhole records is the orientation error that must be corrected for the downhole accelerograph. During this phase, the orientation errors at the depths of 50 m, 100 m and 200 m are finally determined to be 32°, 120° and −84°.

Besides this, particle-motion analysis is used to examine the polarization direction. Figure 4 shows the particle-motion diagrams of two horizontal components of ground displacements at surface and downhole stations for the same event. Arrows mark the directions of the maximum polarization, and the corresponding numbers represent the strikes in degrees. In this analysis, the orientation errors at the depths of 50 m, 100 m and 200 m are found to be 35°, 122° and −88°.

An independent estimation given by CHIU and HUANG (2003a, b), based on the similarity between the synthetic and observed downhole waveforms, shows that the

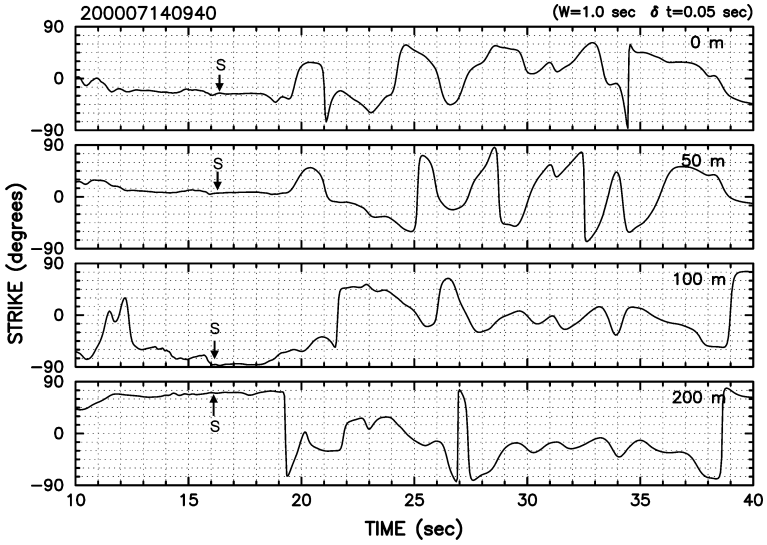

Figure 3
Strike of maximum polarization axes as a function of time for the event of 14 July 2000 (200007140940). From top to bottom, they correspond to the surface, the 50, 100 and the 200 m accelerometers. Arrows mark the primary *S* arrivals, and the corresponding values represent the strikes in degrees.

corresponding orientation errors are 40°, 114° and 284° (or −76°). Although their method shows some superiority, we do not use their result in this paper because its accuracy highly depends on the velocity model.

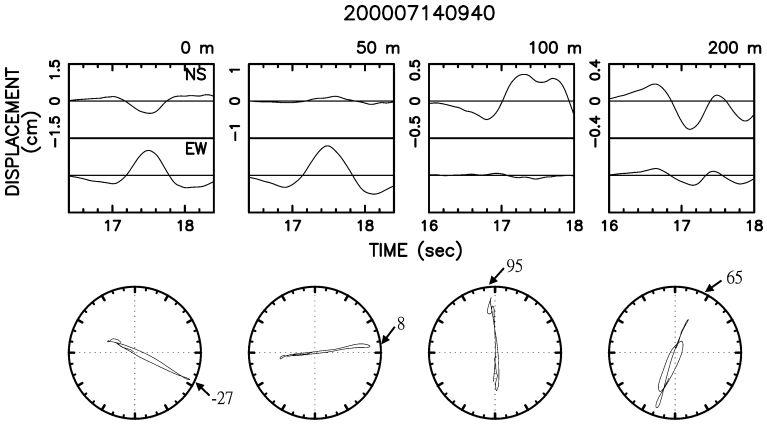

Figure 4
Particle-motion diagrams of the two horizontal components of ground displacements at surface and downhole stations for the event of 14 July 2000 (200007140940). Arrows mark the directions of the maximum polarization, and the corresponding numbers represent the strikes in degrees.

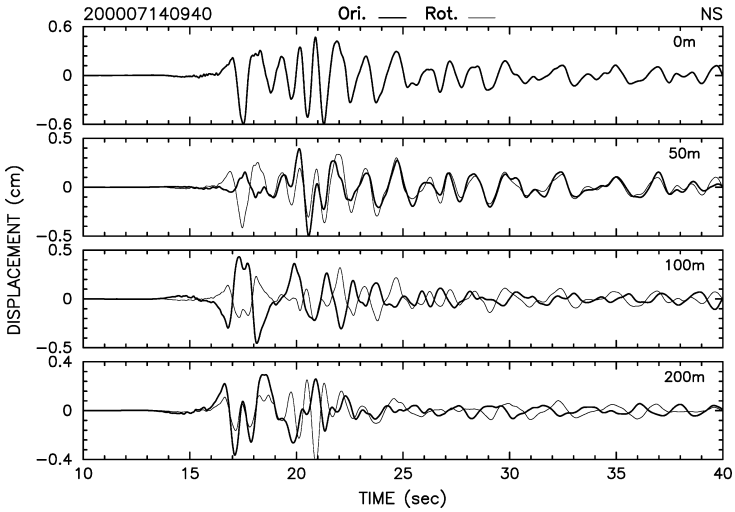

Figure 5
Comparison of waveforms before (thick lines) and after (thin lines) orientation correction for the NS component of the 14 July 2000 earthquake.

Both results of polarization analysis and particle motion are similar. After an overall evaluation, we select the orientation errors determined by polarization analyses to correct all the data used in this study. Figure 5 shows the comparison of waveforms between the before (thick lines) and after (thin lines) orientation corrections for the NS component of the 14 July 2000 earthquake. After the correction, coherency between the surface and downhole records is considerably improved (Fig 6).

4. Spectral Ratio Analysis

In order to study the linear and nonlinear site amplification of the Dahan site, we calculate the spectral ratio at the surface relative to the depths of 50, 100 and 200 m. Figure 7 shows the comparison of site responses for the Chi-Chi earthquake sequence, including the main shock (Event 1) and its three aftershocks (Events $2 \sim 4$) where different line types represent different events. Their PGA values are tabulated in Table 1. It is evident that the main shock event (199909201747, thick lines) has lower predominant frequency (1.66 Hz, 0.95 Hz and 0.68 Hz) than the three aftershock events 199909201757 (1.98 Hz, 1.27 Hz and 0.78 Hz), 199909201811 (1.73 Hz, 1.05 Hz and 0.73 Hz) and 199909201816 (2.03 Hz, 1.17 Hz and 0.83 Hz). The three frequencies in parentheses represent the fundamental predominant frequency at the surface relative to the depths of 50 m,

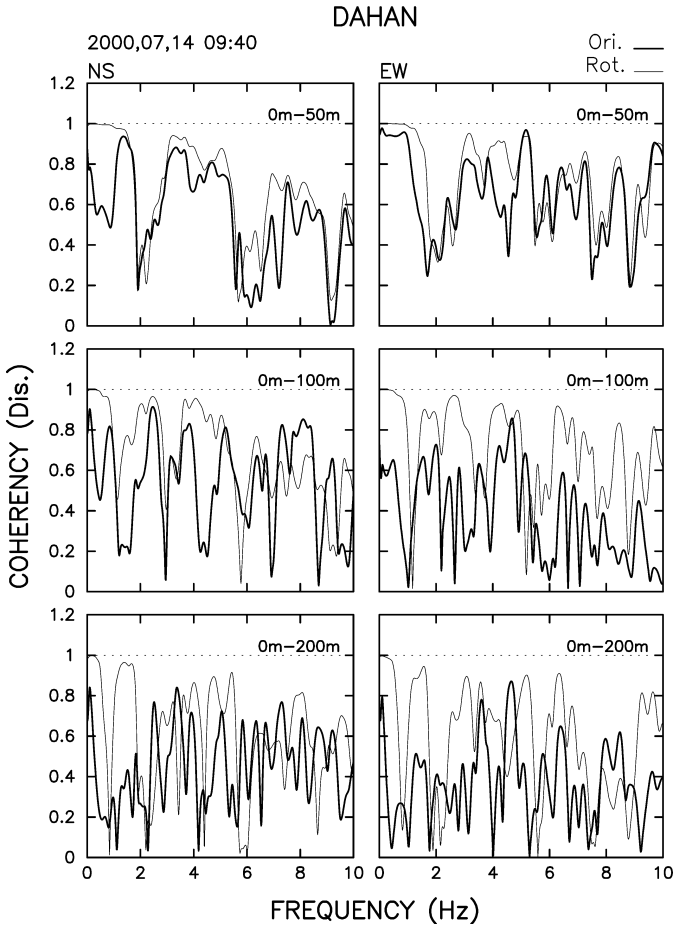

Figure 6
Comparison of coherency function between the surface and downhole records before (thick lines) and after (thin lines) orientation correction for the 14 July 2000 earthquake.

100 m and 200 m for the event. In addition to this, Figure 8 illustrates the strong-motion event (the Chi-Chi main shock, thin lines) compared with the average spectral ratio (thick lines) of four weak-motion events (Events 5–8). The shadow zone represents the means of the weak-motion spectral ratios plus one and minus one standard deviation which corresponds to a 68% confidence interval. For the weak-motion events, the fundamental frequency at 0 m/50 m, 0 m/100 m and 0 m/200 m individually appears at 1.85 Hz, 1.29 Hz and 0.76 Hz. The predominant frequency of the strong-motion event is seen to shift to a lower value. They both indicate that the soil site produced the nonlinear site effect during the Chi-Chi earthquake.

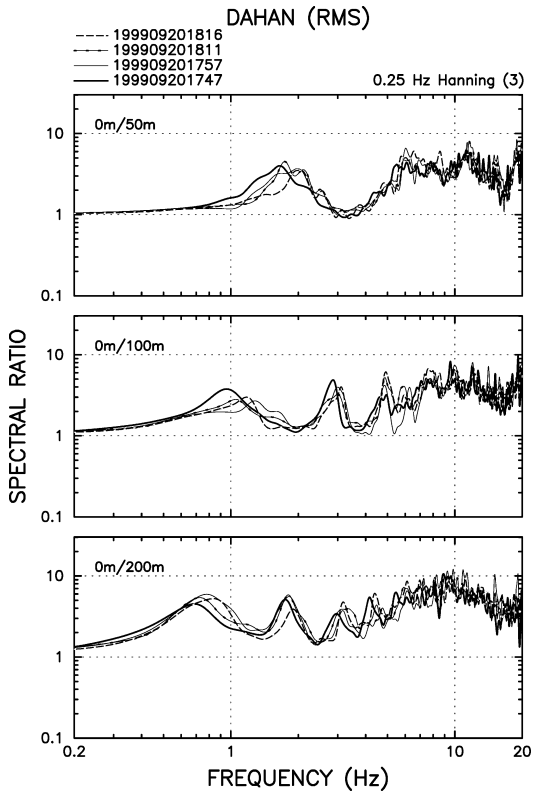

Figure 7
Spectral ratio comparison of the Chi-Chi earthquake sequence including main shock and 3 aftershocks at the depths of 0, 50 and 100 m corresponding to the reference site (200 m). Different line types represent the results of different events.

5. Numerical Simulation

The shallow soil structure around the Dahan downhole array site can be represented by a horizontal layered structure. To study site amplification, we use the Haskell method (HASKELL, 1953, 1960) to simulate the ground motion of the horizontal and layered structure at the Dahan site. The ground motion at surface is chosen as the input to predict the ground motions at the depths of 50 m, 100 m and 200 m (HUANG and CHIU, 1996). The great advantage of this approach is that the upgoing (or direct *S*) wave need not be separated from the downgoing (or reflected) wave. With this technique, the total wavefield corresponding to each layer can be calculated directly. The velocity structures and densities used are listed in Table 2. The velocity structure is divided into 11 layers and is considered to be at the half-space beneath the depth of 200 m. No attenuation term

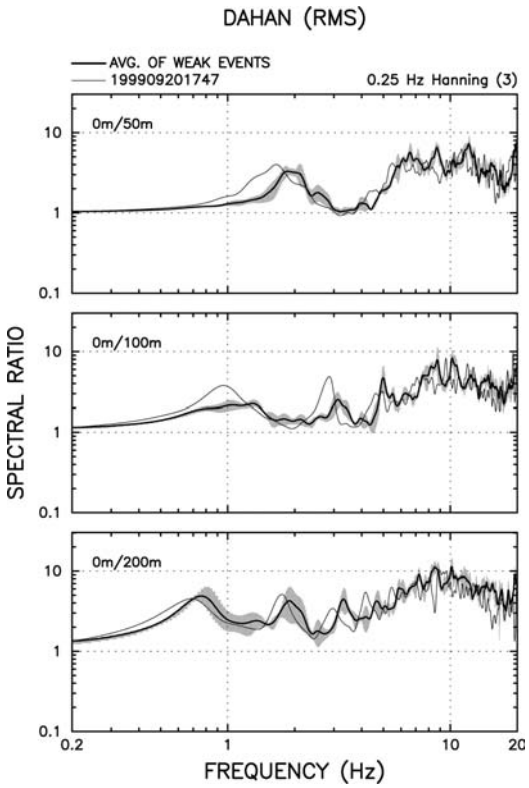

Figure 8
Spectral ratio comparison between the Chi-Chi main shock (thin lines) and the weak-motion events (thick lines) at the depths of 0, 50 and 100 m corresponding to the reference site (200 m). The shadow zone represents the means of the weak-motion spectral ratios plus one and minus one standard deviation which corresponds to a 68% confidence interval.

Table 2

Velocity structure at the Dahan downhole array

Layer No.	Thickness (m)	V_P (m/sec)	V_S (m/sec)	Density (g/cm^3)
1	2	400	133	2.00
2	4.5	1300	231	2.01
3	17.5	2200	398	2.04
4	26	1850	398	2.05
5	11	1850	398	2.05
6	31	1905	454	2.07
7	8	1905	438	2.07
8	6	1905	438	2.07
9	45	1905	500	2.08
10	18	2500	833	2.08
11	31	2500	1050	2.09

$(1/Q_S = 0)$ is added to the simulation process. This is mainly because the propagation distance is short (50 m $\sim$ 200 m) and the bandpass filter used has removed high frequency components which would be most affected by Q_S.

5.1 Simulation of the Weak-Motion Event

Event 5 (199909202147) is selected as one example of the waveform simulation of a weak-motion event. The PGA of this event at the surface is only 18 gals. On the basis of the back-azimuth (238.8°), two horizontal components are used to construct the *SH* wave. All acceleration recordings used are filtered with a bandpass filter (0.05 $\sim$ 8Hz). It is assumed that the *SH* wave is vertically incident from the half-space, and the ground motion at the surface is used to predict the ground motion at downholes. Figure 9 shows the observed (thick lines) and synthetic (thin lines) (a) *SH* displacement and (b) acceleration waveforms of Event 5 based on the velocity model (Table 2). The synthetic waveforms at the depths of 50 m, 100 m and 200 m closely match the observed waveforms both in terms of amplitude and phase. The simplified model provides a good simulation for the weak-motion recordings.

5.2 Simulation of the Chi-Chi Earthquake Sequence

The Chi-Chi earthquake induced strong shaking and caused heavy damage in Taiwan. To investigate whether the nonlinear effect of soil occurred at the Dahan site during the Chi-Chi earthquake, we perform simulations using the Haskell method for the Chi-Chi earthquake sequence (Events 1–4 in Table 1).

Figure 10 presents the comparison of the observed (thick lines) and synthetic (thin lines) *SH* waveforms, including (a) acceleration and (b) displacement, of the Chi-Chi main shock (Event 1) based on the velocity model given in Table 2. It is apparent that the synthetic waveforms do not match the observed data well with respect to the phase. For the *S*-wave part (18.5–25.5 sec), the synthetic amplitudes are underestimated, while their phases arrive earlier than those in the observed data. This means that the nonlinear site effect is observed, and it reduced the shallow velocity structure during the Chi-Chi main shock. It is likely the soil property changed during the period of strong shaking.

About ten minutes after the main shock (Event 1), an aftershock (Event 2) occurred. Figure 11 shows the synthetic results (thin lines) compared with the observed data (thick lines). The arrival time of the *S* waves is about 16.5 sec. Although the ground motion (PGA = 87gals) is not very large at the Dahan site, the linear model still cannot reproduce the observed waveform. The nonlinear behavior like the lower amplitude and earlier phase also appears in the simulated results. The phenomenon probably can be explained by the fact that the return time, only 10 minutes, was too short for it to revert to the initial state of the soil since the aftershock followed closely.

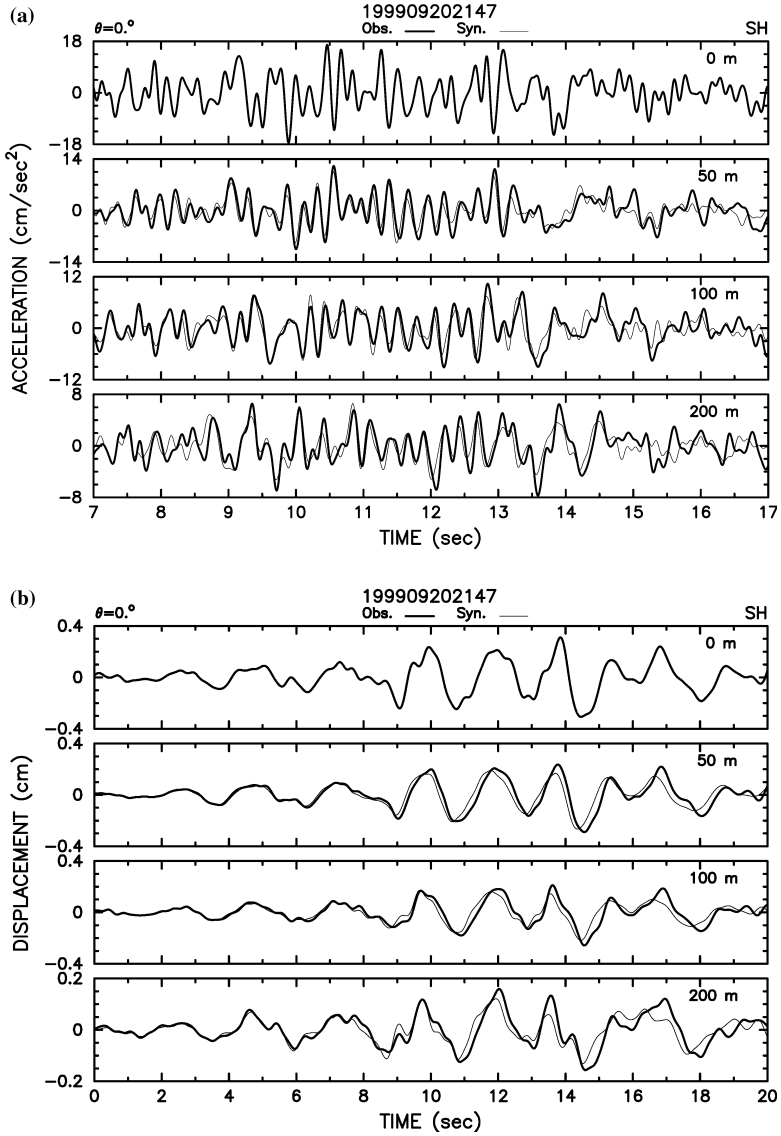

Figure 9
Observed (thick lines) and synthetic (thin lines). (a) SH acceleration and (b) displacement waveforms of the 20 September 1999 earthquake (199909202147) based on the velocity model (Table 2). The SH wave is vertically incident from the half-space (200 m). Both match well.

About 14 minutes after Event 2, another aftershock (Event 3) occurred. It was a strong-motion event (PGA = 166gals). Figure 12 shows the synthetic results (thin lines) compared with the observed data (thick lines). The arrival time of the *S* wave was about 16 sec. For the *S*-wave part, the synthetic amplitude and phase arrivals are

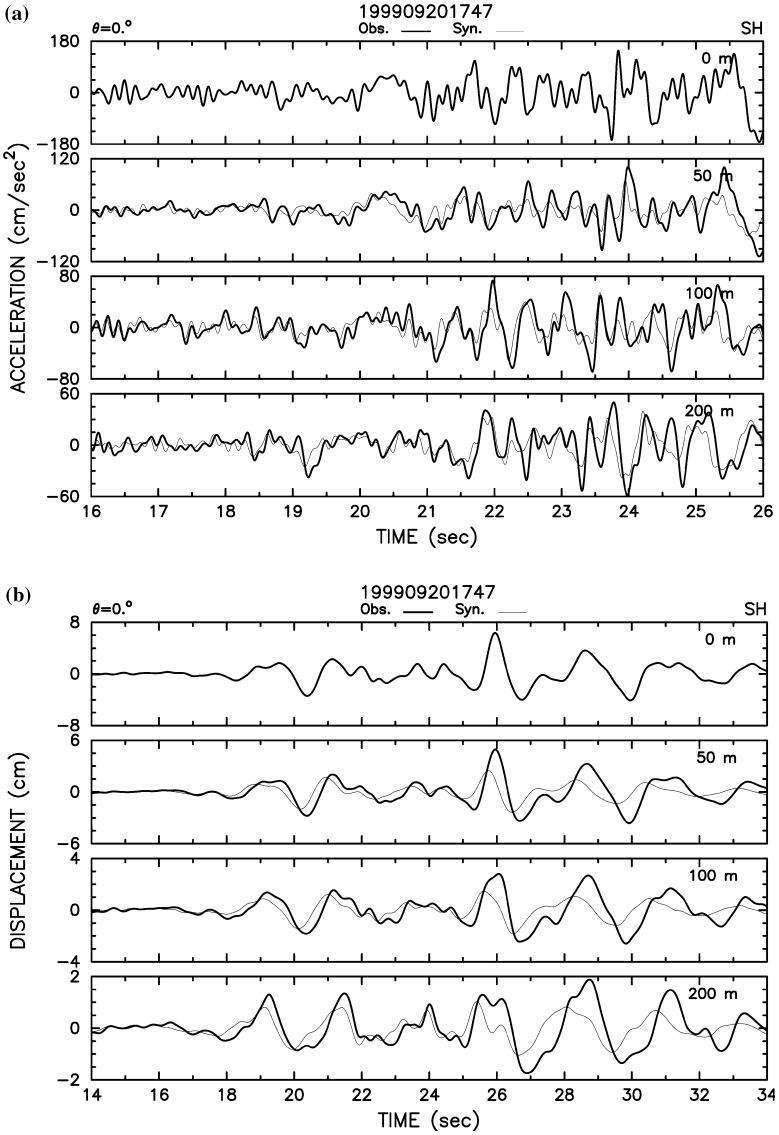

Figure 10
Observed (thick lines) and synthetic (thin lines). (a) *SH* acceleration and (b) displacement waveforms of the 20 September 1999 main shock (Event No.1, 199909201747) based on the velocity model (Table 2).

still smaller and earlier than the observed one. Aside from this, according to the spectral ratio analysis (dotted-thin lines in Fig. 7), the site shows lower predominant frequency for the event. They both demonstrate that the site was still on the nonlinear status at that time.

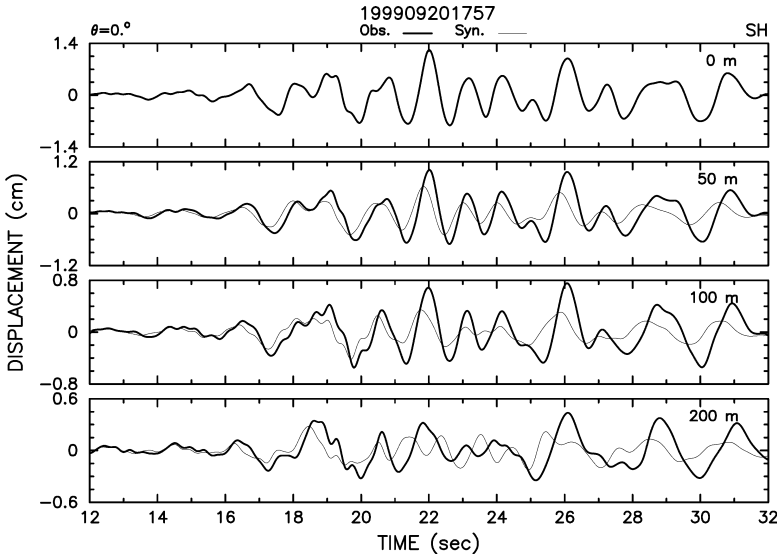

Figure 11
Observed (thick lines) and synthetic (thin lines) *SH* waveforms of the 20 September 1999 aftershock (Event No.2, 199909201757) based on the velocity model (Table 2).

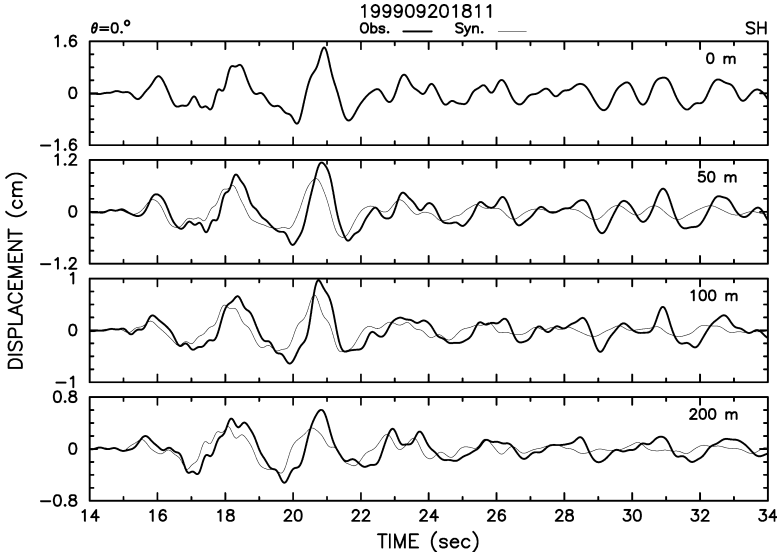

Figure 12
Observed (thick lines) and synthetic (thin lines) *SH* waveforms of the 20 September 1999 aftershock (Event No.3, 199909201811) based on the velocity model (Table 2).

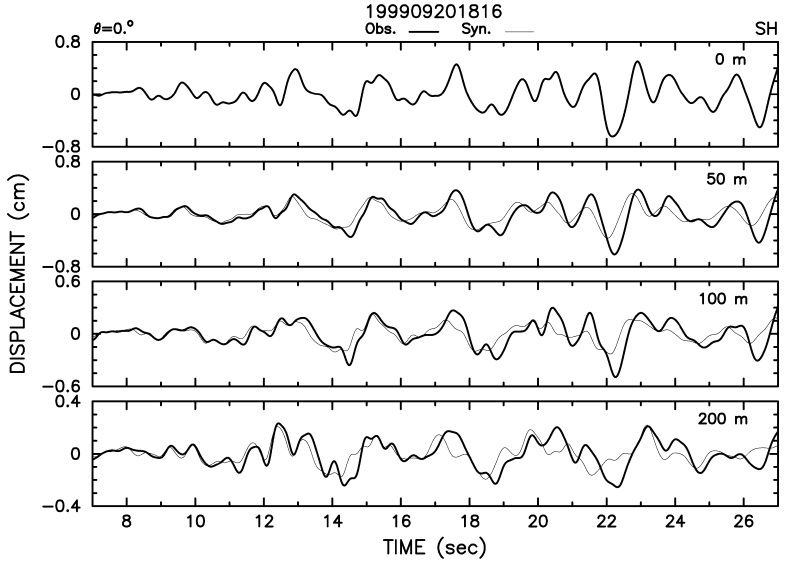

Figure 13
Observed (thick lines) and synthetic (thin lines) *SH* waveforms of the 20 September 1999 aftershock (Event No. 4, 199909201816) based on the velocity model (Table 2). Both match well in terms of amplitude and phase.

About five minutes after Event 3, another aftershock (Event 4) took place. It was nearly a weak-motion event although its PGA value (PGA = 68 gals) at surface is slightly larger than the weak-motion threshold. Figure 13 presents the synthetic results (thin lines) compared with the observed data (thick lines). The arrival time of the *S* waves was about 8 sec. For Event 4, the Haskell method using the velocity model (Table 2) produces a good simulation. The synthetic waveform matches well with the observed data both in amplitude and phase. This means that the soil site recovered to the linear state as soon as the event occurred.

In order to further demonstrate the evolution of the nonlinear behavior of soil within the first half hour after the main shock at the Dahan downhole site, we plot the change of the fundamental predominant frequency (F_p), and its amplification factor (A_p) in Figures 14(a) and (b). The corresponding PGA values are shown in Figure 14(c). Apparently, Event 1 (main shock) has the lowest predominant frequency at 0 m/50 m, 0 m/100 m and 0 m/200 m while it has the maximum PGA value at different depths. Furthermore, the synthetic result using the linear model fails to fit the observation (Fig. 10). These two facts indicate that the large ground motion has caused the nonlinear behavior of soil. Similar results are also found in Event 3. The predominant frequency of Event 2 is abnormal. Although its PGA is only 87 gals, this event has a lower predominant frequency. One possible explanation is that the soil condition did not return to its normal

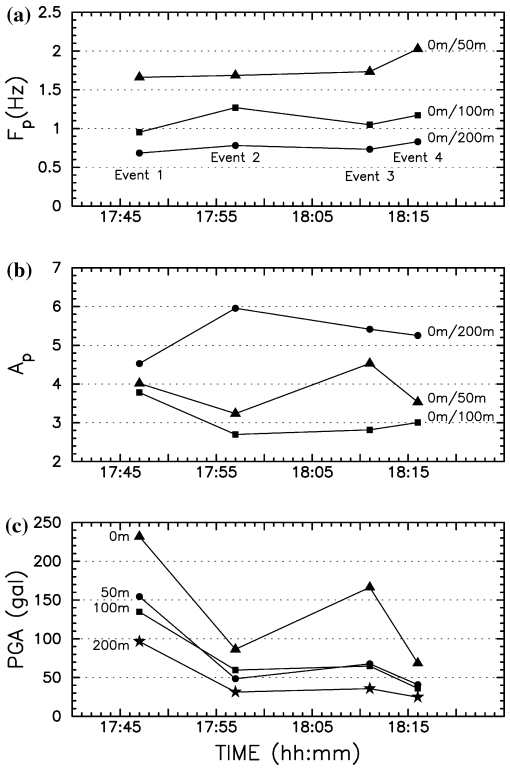

Figure 14
The changes of (a) the fundamental predominant frequency (F_p), and (b) its corresponding amplification factor (A_p) with time within the first half-hour after the main shock (Event 1). The PGA of these data is shown in (c).

state after 10 minutes of the main shock. Moreover, the predominant frequency of Event 4 has gradually returned to the normal state while its ground motion is not large (PGA = 68 gals). This indicates that the soil condition was recovering after 30 minutes of the main shock. As regards the amplification factor (A_p) shown in Figure 14(b), it seems that the recovery is not sensitive to this parameter. It is difficult to detect its systematic change during the first half hour of the main shock.

6. Conclusions

The four-level array (0 m, 50 m, 100 m and 200 m) is located to the north of Hualien City in eastern Taiwan. In this paper, the site characteristics of the Dahan downhole array are studied by analyzing the recordings of the Chi-Chi earthquake

sequences. Polarization and particle-motion analyses are used to check the orientation errors of the seismometers at three different depths. The orientation errors of the downhole instruments at the depths of 50 m, 100 m and 200 m are 32°, 120° and −84°.

All of the recordings used involve orientation corrections. We calculate the spectral ratios at the surface corresponding to the depths of 50 m, 100 m and 200 m. For the Chi-Chi earthquake sequence, the main shock apparently had a lower dominant frequency than the three aftershocks observed. Additionally, the predominant frequency of the Chi-Chi main shock shifted to a lower frequency when compared with the weak-motion events.

The ground motion at the surface is used to predict ground motions at downholes, by assuming that the *SH* wave is vertically incident from the half-space. According to the synthetic results, unlike the weak-motion event which can be reproduced, the strong-motion event cannot be reproduced well. For the Chi-Chi earthquake sequence (Events 1–4 in Table 1), the linear Haskell model cannot predict well the ground motion except Event 4, indicating that the nonlinear effect was induced at the Dahan site during the strong shaking of the Chi-Chi earthquake.

Acknowledgements

The authors would like to express their thanks to Dr. L.F. Bonilla and one anonymous reviewer for their valuable suggestions. This research was supported by the National Science Council under grant number NSC 89-2921-M-194-007. The Institute of Earth Sciences, Academia Sinica supplied the strong-motion data. The support of these organizations is gratefully acknowledged.

References

Aki, K. and Irikura, K. (1991), *Characterization and mapping of earthquake shaking for seismiczonation*, in *Proc. 4th Intl. Conf. On Seismic Zonation*, Vol. 1, pp 61–110.

Aguirre, J., Irikura, K., and Kudo, K. (1994), *Estimation of strong ground motions on hard rock and soft sediment sites in the Ashigara Valley using the empirical Green's function method, Bull. Disas. Prev. Res. Inst., Kyoto Univ.*, Vol. 44, Part1, No. 379, pp. 45–68.

Aguirre, J. and Irikura, K. (1995), *Preliminary Analysis of Nonlinear Site Effects at Port Island Vertical Array Station during the 1995 Hyogoken-Nanbu Earthquake*, J. Natural Disas. Sci. *16*, 49–58.

Aguirre, J. and Irikura, K. (1997), *Nonlinearity, Liquefaction, and Velocity Variation of Soft Soil Layers in Port Island, Kobe, during the Hyogoken-Nanbu Earthquake*, Bull. Seismol. Soc. Am. *87*, 1244–1258.

Beresnev, I.A., Wen, K.L., and Yeh, Y.T. (1995a), *Nonlinear Soil Amplification: Its Corroboration in Taiwan,* Bull. Seismol. Soc. Am. *85*, 496–515.

Beresnev, I.A., Wen, K.L., and Yeh, Y.T. (1995b), *Seismological Evidence for Nonlinear Elastic Ground Behavior during Large Earthquakes*, Soil Dyn. Earthquake Eng. *14*, 103–114.

BERESNEV, I.A., ATKINSON, G.M., JOHNSON, P.A., and FIELD, E.H. (1998a), *Stochastic Finite-fault Modeling of Ground Motions from the 1994 Northridge, California, Earthquake. II. Widespread Nonlinear Response at Soil Sites,* Bull. Seismol. Soc. Am. *88*, 1402–1410.

BERESNEV, I.A., FIELD, E.H., ABEELE, K.V. D., and JOHNSON, P.A. (1998b), *Magnitude of Nonlinear Sediment Response in Los Angeles Basin during the 1994 Northridge, California, Earthquake,* Bull. Seismol. Soc. Am. *88*, 1079–1084.

BORJA, R.I. and WU, W.H. (1994), *Vibration of Foundations on Incompressible Soils with no Elastic Region*, J. Geotech. Engin., ASCE *120*, 1570–1592.

BORJA, R.I., CHAO, H.Y., MONTANS, F.J., and LIN, C.H. (1999), *Nonlinear ground response at Lotung LSST site*, J. Geotech. Geoenviron. Engin. *125*, 187–197.

BORJA, R.I., LIN, C.H., SAMA, K.M., and MASADA, G.M. (2000), *Modelling Nonlinear Ground Response of Non-liquefiable Soils*, Earthq. Engin. Struct. Dyn. *29*, 63–83.

CHIN, B.H. and AKI, K. (1991), *Simultaneous Study of the Source, Path, and Site Effects on Strong Ground Motion during the 1989 Loma Prieta Earthquake: a Preliminary Result on Pervasive Nonlinear Site Effects*, Bull. Seismol. Soc. Am. *81*, 1859—1884.

CHIU, H.C., HUANG, H.C., LEU, C.L., and NI, S.D. (1994), *Application of Polarization Analysis in Correcting the Orientation Error of Downhole Seismometers*, Earthq. Engin. Struct. Dyn. *23*, 1069–1078.

CHIU, H.C. and HUANG, H. C. (2003a), *Estimating the Orientation Error of the Dahan Downhole Accelerometer Using the Maximum Cross-correlation Coefficient between the Observed and Synthetic Waves*, J. Seismol. 7, 493–505.

CHIU, H.C. and HUANG, H.C. (2003b), *An Effective Algorithm to Correct the Orientation Error and Time Shift of Downhole Seismograms*, TAO, *2*, 133–144.

CULTRERA, G., BOORE, D.M., JOYNER, W.B., and DIETEL, C.M. (1999), *Nonlinear Soil Response in the Vicinity of the Van Norman Complex following the 1994 Northridge, California, Earthquakes*, Bull. Seismol. Soc. Am. *89*, 1214–1231.

ELGAMAL, A.W., ZEGHAL, M., PARRA, M., GUNTURI, R., TANG, H.T., and STEPP, J.C. (1996), *Identification and Modeling of Earthquake ground Response – I. Site Amplification*, Soil Dyn. Earthq. Engin. *15*, 499–522.

HASKELL, N.A. (1953), *The Dispersion of Surface Waves on Multilayered Media*, Bull. Seismol. Soc. Am. *43*, 17–35.

HASKELL, N.A. (1960), *Crustal Reflection of Plane SH Waves*, J. Geophys. Res. *65,* 4147–4150.

HARTZELL, S. (1998), *Variability in Nonlinear Sediment Response during the 1994 Northridge, California, Earthquake,* Bull. Seismol. Soc. Am. *88*, 1426–1437.

HUANG, H.C., and CHIU, H.C. (1996), *Estimation of Site Amplification from Dahan Downhole Recordings*, Earthq. Eng. Struct. Dyn*, 25*, 319–332.

JOYNER, W.B. and CHEN, A.T.F. (1975), *Calculation of Nonlinear Ground Response in Earthquake*, Bull. Seismol. Soc. Am. *65*, 1315–1336.

LEE, M.K.W. and FINN, W.D.L. (1982), *Dynamic effective stress response analysis of soil deposits with energy transmitting boundary including assessment of liquefaction potential*, *Rev., Dep. Civil Eng., Soil Mechanics Series* No. 38, the Univ. of British Columbia, Vancouver, Canada.

NI, S.D., SIDDHARTHAN, R.V., and ANDERSON J.G. (1997), *Characteristics of Nonlinear Response of Deep Saturated Soil Deposits*, Bull. Seism. Soc. Am. *87*, 342–355.

ORDAS, M. and FACCIOLI, E. (1994), *Site Response Analysis in the Valley of Mexico: Selection of Input Motion and Extent of Nonlinear Soil Behavior*, Earthq. Engin. Struct. Dyn*, 23*, 895–908.

SATOH, T., SATO, T., and KAWASE, H. (1995), *Nonlinear Behavior of Soil Sediments Identified by Using Borehole Records Observed at Ashigara Valley, Japan*, Bull. Seismol. Soc. Am. *85*, 1821–1834.

SCHNABEL, P.B., LYSMER, J., and SEED, H.B. (1972), *SHAKE: A computer program for earthquake response analysis of horizontally layered sites*, *Report EERC* 72–12, Earthquake Engineering Research Center, University of California, Berkeley.

STREETER, V.L., WYLIE, E.B., and RICHART, F.E. (1974), *Soil Motion Computation by Characteristic Method,* J. Geotech. Eng. Div. ASCE *100*, 247–263.

SU, F., ANDERSON, J.G., and ZENG, Y. (1998), *Study of Weak and Strong Ground Motion Including Nonlinearity from the Northridge, California, Earthquake Sequence*, Bull. Seismol. Soc. Am. *88*, 1411–1425.

WEN, K.L., BERESNEV, I.A., and YEH, Y.T. (1994), *Nonlinear Soil Amplification Inferred from Downhole Strong Seismic Motion Data*, Geophys. Res. Lett. *21*, 2625–2628.

WEN, K.L., BERESNEV, I.A., and YEH, Y.T. (1995), *Investigation of Nonlinear Site Amplification at Two Downhole Strong Ground Motion Arrays in Taiwan,* Earthq. Eng. Struct. Dyn. *24*, 313–324.

YU, G., ANDERSON, J.G., and SIDDHARTHAN, R. (1993), *On the Characteristics of Nonlinear Soil Response*, Bull. Seism. Soc. Am. *83*, 218–244.

(Received 6 November, 2002, accepted 26 August, 2003)